



This is the accepted manuscript made available via CHORUS. The article has been published as:

Dipole-obstructed Cooper pairing: Theory and application to math xmlns="http://www.w3.org/1998/Math/MathML">mrow>mi>j/mi>mo>=/mo>mfrac>mn>3/mn>mn>2/mn>/mfrac>/mrow>/math> superconductors

Penghao Zhu and Rui-Xing Zhang

Phys. Rev. B **111**, L081107 — Published 12 February 2025

DOI: 10.1103/PhysRevB.111.L081107

Dipole-Obstructed Cooper Pairing: Theory and Application to $j = 3/2$ Superconductors

Penghao Zhu[1,*] and Rui-Xing Zhang[2,3,†]

[1] *Department of Physics, The Ohio State University, Columbus, OH 43210, USA*
[2] *Department of Physics and Astronomy, The University of Tennessee, Knoxville, TN 37996, USA*
[3] *Department of Materials Science and Engineering, The University of Tennessee, Knoxville, TN 37996, USA*

Like electrons, Cooper pairs can carry a monopole charge if the pairing electrons come from two or more Fermi surfaces with different Chern numbers. In such an instance, a superconductor is necessarily nodal due to an inherent topological pairing obstruction. In this work, we show that a similar obstruction is also possible when there is only one Fermi surface involved in the pairing process. By developing a Chern-vorticity theorem, we have identified a class of Fermi surfaces with a quantized dipolar Berry flux pattern, where all intra-Fermi-surface Cooper pairings are "dipole-obstructed" and nodal. As a real-world application, we find that the dipole obstruction plays a crucial role in stabilizing the superconducting nodal structure for $j = 3/2$ half-Heusler compounds.

Introduction.— Superconductors (SCs) are generally classified by the symmetry pattern of their Cooper pairs. By definition, electron pairing in a conventional s-wave SC is spatially isotropic, generating a uniform energy gap of the normal-state Fermi surface (FS) [1]. Meanwhile, an unconventional SC such as the cuprates can feature a gapless spectrum when its anisotropic pairing order $\Delta(\mathbf{k})$ has symmetry-enforced zeros in the momentum space [2–4]. In experiments, the SC gap structure can be feasibly probed by angle-resolved photoemission spectroscopy [5], scanning tunneling spectroscopy [6], penetration depth measurements [7], etc. Such gap information often offers valuable insights into unraveling the nature of Cooper pairs for a new SC candidate.

The pairing symmetry, however, does not fully account for the gap structure of SCs. For example, a SC is found to be necessarily nodal, once the electrons forming a Cooper pair come from two FSs with opposite Berry monopole charges [8–11]. Such an inability to develop a full energy gap is intrinsic to the topological texture of the FS, which holds even when $\Delta(\mathbf{k})$ is constant. This striking phenomenon has sparked a growing research interest in uncovering similar mechanisms of topologically obstructed nodal pairing orders for FSs carrying an Euler index [12–14] or a $\mathbb{Z}_2$ index [15]. Notably, most existing theories have assumed the obstructed pairings to involve multiple FSs, while generalizations to intra-FS electron pairings are less explored.

In this work, we have identified a new class of FSs where all intra-FS Cooper pairings exhibit topology-enforced zeros. The FS of our interest encloses a quantized dipole of the Berry curvature [16], i.e., there exists a Berry flux of $\pm 2\pi$ through either half of the FS, while the net Berry flux vanishes. As a proof of concept, we consider a minimal model with such a Berry-dipole FS and find all intra-FS Cooper pairings are *dipole-obstructed* from fully gapping out the FS. Specifically, the resulting SC state always exhibits zero-energy Weyl nodes and/or nodal loops in the Bogoliubov-de Gennes (BdG) spectrum. Finally, we revisit the half-Heusler SCs such as YPtBi [4, 17] and LuPdBi [18–20], which are believed to feature a mixed-parity singlet-septet pairing [21]. We find that the dipole obstruction naturally exists in the septet pairing channel and further clarify its contribution to the BdG line nodes observed in experiments.

Chern-Vorticity Theorem and Pairing Zeros.— We start by presenting a Chern-vorticity theorem that will guide us to the target FSs. As shown in Fig. 1(a), we consider two 2D closed or *effectively* closed manifolds $\mathcal{M}_1$ and $\mathcal{M}_2$ in $\mathbf{k}$-space, as well as two Bloch states $|\psi_1(\mathbf{k}_1)\rangle$ and $|\psi_2(\mathbf{k}_2)\rangle$ with $\mathbf{k}_i \in \mathcal{M}_i$. Here, we define an open manifold to be effectively closed if the Bloch states over each of its boundaries are identical. Generally, $\mathcal{M}_1$ and $\mathcal{M}_2$ are related by a $\mathbf{k}$-space transformation $\{g|\mathbf{t}\}$ with $\mathbf{k}_2 = g\mathbf{k}_1 + \mathbf{t}$. Here g denotes a point-group operation (e.g., rotation and mirror) that satisfies $g^{-1} = g^T \in \mathbb{R}$ and $\mathbf{t}$ is a translation in $\mathbf{k}$-space. We now consider the matrix element of a general two-particle operator $\hat{O}$ describing quadratic electron-electron/electron-hole couplings between electrons/holes with momenta on $\mathcal{M}_1$ and $\mathcal{M}_2$:

$$\mathcal{O}(\mathbf{k}_1) = \langle\psi_1(\mathbf{k}_1)|\hat{O}|\psi_2(\mathbf{k}_2)\rangle = |\mathcal{O}(\mathbf{k}_1)|e^{i\varphi(\mathbf{k}_1)}. \quad (1)$$

When φ displays a vortex pattern around $\mathbf{k}_1 = \mathbf{k}_{v_i}$, the value of $\mathcal{O}(\mathbf{k}_{v_i})$ necessarily vanishes and is thus topologically obstructed. Such a vortex v_i is captured by a vorticity index around $\mathbf{k}_{v_i}$, defined as $\nu_i = 1/(2\pi)\oint d\mathbf{k}_1 \cdot \partial_{\mathbf{k}_1}\varphi(\mathbf{k}_1) \in \mathbb{Z}$, where the integral is over an infinitesimal loop surronding $\mathbf{k}_{v_i}$. The Chern-vorticity theorem proven in the Supplemental Material (SM) [22] dictates that the net vorticity on $\mathcal{M}_1$, $\nu = \sum_i \nu_i \in \mathbb{Z}$, is determined by

$$\begin{aligned} \nu &= \mathcal{C}_1 - (\det g)\mathcal{C}_2 + \mathcal{I}_\varphi, \\ \mathcal{I}_\varphi &= \sum_{\partial\mathcal{M}_1} \oint_{\partial\mathcal{M}_1} \frac{d\mathbf{k}_1}{2\pi} \cdot \partial_{\mathbf{k}_1}\varphi(\mathbf{k}_1), \end{aligned} \quad (2)$$

* zhu.3711@osu.edu
† ruixing@utk.edu

where $\mathcal{C}_\alpha$ is the single-particle Chern number of $|u_\alpha(\mathbf{k}_\alpha)\rangle \equiv e^{-i\mathbf{k}_\alpha\cdot\mathbf{r}_\alpha}|\psi_2(\mathbf{k}_\alpha)\rangle$ on $\mathcal{M}_\alpha$. The loop integral $\mathcal{I}_\varphi$ is summed over all possible boundaries of $\mathcal{M}_1$, which, by default, vanishes for a closed $\mathcal{M}_1$. The essential idea of the Chern-vorticity theory is that the phase of $\mathcal{O}(\mathbf{k}_1)$ can be linked to the Berry connections $\mathbf{A}_a(\mathbf{k}_a) = i\langle\psi_a(\mathbf{k}_a)|\partial_{\mathbf{k}_a}\psi_a(\mathbf{k}_a)\rangle$ on $\mathcal{M}_{a=1,2}$ by constructing a gauge invariant vector:

$$\mathbf{S} = \partial_{\mathbf{k}_1}\varphi(\mathbf{k}_1) - \mathbf{A}_1(\mathbf{k}_1) + g^T\mathbf{A}_2(\mathbf{k}_2). \tag{3}$$

If there is a nonzero Chern-number of $|\psi_1(\mathbf{k_1})\rangle$ ($|\psi_2(\mathbf{k_2})\rangle$) on effectively closed $\mathcal{M}_1$ ($\mathcal{M}_2$), then $\mathbf{A}_1(\mathbf{k}_1)$ ($\mathbf{A}_2(\mathbf{k}_2)$) must be singular somewhere on the manifold. Around the singularity of the Berry connections, one can always choose a gauge such $\mathbf{S}$ is smooth. Consequently, there must be a singularity in $\partial_{\mathbf{k}_1}\varphi(\mathbf{k}_1)$ to cancel that of Berry connections. This establishes the connection between the vorticity of $\mathcal{O}(\mathbf{k}_1)$ and the Chern number over $\mathcal{M}_1$ and $\mathcal{M}_2$ manifested in Eq. (2). The boundary term I_φ arises because, while $|\psi_{1,2}(\mathbf{k}_{1,2})\rangle$ remain constant quantum states along the boundaries of effectively closed manifold $\mathcal{M}_{1,2}$, $\mathcal{O}(\mathbf{k}_1)$ can generally have nontrivial momentum-dependence along the boundaries. The detailed technical proof can be found in the Supplemental Material (SM) S1 [22] .

Focusing on SCs, we choose $|\psi_1(\mathbf{k}_1)\rangle = |\xi_1^{(e)}(\mathbf{k}_1)\rangle$ and $|\psi_2(\mathbf{k}_2)\rangle = |\xi_2^{(e)\star}(\mathbf{k}_2)\rangle$ in order to properly project the pairing operator $\hat{O}$, since $\hat{O}$ physically describes hoppings between electrons and holes. Here, $|\xi_\alpha^{(e)}(\mathbf{k}_\alpha)\rangle$ is the Bloch state of electrons on the Fermi surface $\mathcal{M}_\alpha$, and $|\xi_\alpha^{(e)\star}(\mathbf{k}_\alpha)\rangle$ is the complex conjugate of $|\xi_\alpha^{(e)}(\mathbf{k}_\alpha)\rangle$. It is crucial to note that $\mathcal{C}_2$, the Chern number for $|\psi_2(\mathbf{k}_2)\rangle$, is exactly opposite to $\mathcal{C}_2^{(e)}$, the electronic Chern number for $|\xi_2^{(e)}(\mathbf{k}_2)\rangle$ on $\mathcal{M}_2$ [22]. As a concrete example, we immediately arrive at $\nu = 2$ when (i) $\mathcal{M}_{1,2}$ are both closed FSs with $\mathcal{C}_1 = \mathcal{C}_2 = +1$ and (ii) g is the spatial inversion with $\det g = -1$, which exactly corresponds to the obstructed nodal pairing for monopole SCs in Ref. [9]. Therefore, the Chern-vorticity theorem manifests as a natural generalization of Ref. [9], but its application transcends the realm of SC systems with inter-FS pairings [23–25].

Berry-Dipole Fermi Surface.— The above Chern-vorticity theorem suggests that for a single Fermi surface $\mathcal{M} \equiv \mathcal{M}_+ \cup \mathcal{M}_-$, the intra-FS pairing between two patches $\mathcal{M}_\pm$ can be topologically obstructed if each patch is effectively closed and carries a nonzero quantized Berry flux. Further requiring the net Berry flux to be zero, we are thus looking for a FS with a quantized dipolar texture of Berry curvature, i.e., a Berry-dipole FS [16, 26–29].

As discussed in Refs. [16, 26] and reviewed in the SM [22], quantization of a Berry-dipole can be achieved by enforcing a mirror symmetry along the dipole axis. As a concrete example, we consider a minimal model with Berry-dipole physics proposed in Ref. [16],

$$h_0 = 2k_z(k_x\sigma_x + k_y\sigma_y) + (k_x^2 + k_y^2 - k_z^2 + \Sigma)\sigma_z. \tag{4}$$

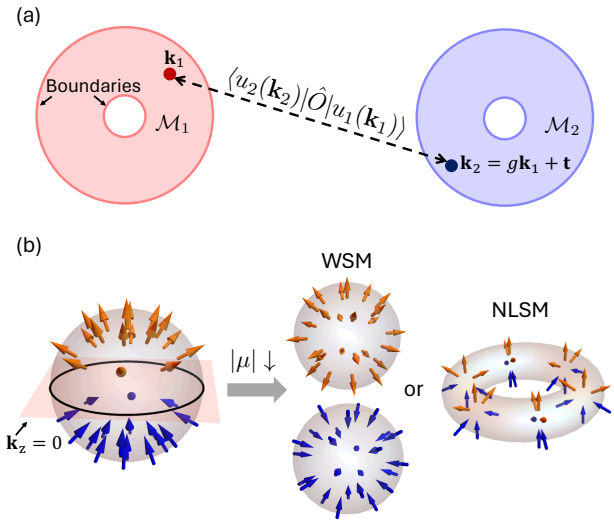


FIG. 1. (a) The Chern-vorticity theorem informs the phase vortex of $\hat{O}$ when projecting onto two closed or effectively closed manifolds $\mathcal{M}_{1,2}$. (b) Berry-dipole FSs for h_0, where the arrows denote the Berry curvature vectors on the FS. A change of μ or Σ can modify the FS topology, while the quantization of Berry dipole always remains robust.

Besides mirror symmetry along z-direction $M_z = i\sigma_z$, h_0 respects a continuous rotation symmetry around z with $C_\theta = \exp[-iJ_z\theta]$, where $J_z = \mathrm{diag}(3/2, 1/2)$ is a diagonal matrix. Lattice regularizing h_0 will reduce the symmetry group to C_{4h}, which will be exploited for later pairing analysis. When $\Sigma > 0$, h_0 describes a 3D minimal Weyl semimetal (WSM) with two Weyl nodes at $k_z = \pm\sqrt{\Sigma}$, respectively. At $\Sigma = 0$, the Weyl nodes merge at Γ to form a quadratic band touching. The annihilation of Weyl nodes, however, does not lead to a mass generation for the low-energy electrons. Instead, we note that h_0 with $\Sigma < 0$ features a 1D doubly degenerate nodal loop in the $k_z = 0$ plane, i.e., a nodal-loop semimetal (NLSM). This unexpected robustness of Weyl nodes arises from the Berry-dipole *delicate* topological charges [16, 26].

Let us generally denote the FS patch with $k_z > 0$ ($k_z < 0$) as $\mathcal{M}_+$ ($\mathcal{M}_-$). For $|\mu| > |\Sigma|$, we always find a single spherical-like FS $\mathcal{M}$ regardless of the value of Σ, where $\mathcal{M}_+$ and $\mathcal{M}_-$ are hence the north and south hemispheres, respectively. Undergoing the Lifshitz transition with $|\mu| < |\Sigma|$, the WSM with $\Sigma > 0$ comprises a pair of closed spherical FSs (i.e., $\mathcal{M}_\pm$), while a single torus-like FS is found for the NLSM ($\Sigma < 0$) with $\mathcal{M}_\pm$ now being both open and of an annulus shape. Evidently, the boundaries of $\mathcal{M}_+$ and $\mathcal{M}_-$, if present, are always sitting in the $k_z = 0$ plane regardless of Σ. Consequently, the eigenstates of h_0 along each boundary can always be uniform, owing to the M_z symmetry. Hence, we conclude that $\mathcal{M}_+$ and $\mathcal{M}_-$ must be either closed or effectively closed for all choices of μ and Σ. This guarantees the FS(s) of h_0 to always feature a quantized Berry dipole,

as explicitly confirmed in Fig. 1(b).

Dipole-Obstructed Pairing.— We are now ready to explore Cooper pairing physics on the above Berry-dipole FS by updating h_0 to a BdG Hamiltonian,

$$H(\mathbf{k}) = \begin{pmatrix} h_0(\mathbf{k}) - \mu & \Delta(\mathbf{k}) \\ \Delta^\dagger(\mathbf{k}) & \mu - h_0^T(-\mathbf{k}) \end{pmatrix}. \tag{5}$$

The pairing matrix generally takes the form $\Delta(\mathbf{k}) = d_0(\mathbf{k})\sigma_0 + \mathbf{d}(\mathbf{k}) \cdot \boldsymbol{\sigma}$ and the Fermi statistics requires $\Delta(\mathbf{k}) = -\Delta^T(-\mathbf{k})$. For our purpose, we consider expanding $d_i(\mathbf{k})$ up to $\mathcal{O}(\mathbf{k}^2)$ and classify all pairing channels based on the irreducible representations (irreps) of C_{4h} group in Table. I [22]. For $|\mu| > |\Sigma|$, $\Delta(\mathbf{k})$ describes the intra-FS pairings (as there is only one FS). Following Eq. 1, the projected Cooper pairing onto $\mathcal{M}_\pm$ is given by $\Delta_{\text{eff}} = \langle \xi_+^{(e)}(\mathbf{k})|\Delta(\mathbf{k})|\xi_-^{(e)\star}(-\mathbf{k})\rangle$, where $|\xi_\pm^{(e)}\rangle$ are normal states over $\mathcal{M}_\pm$.

We first note that a pairing with $\mathcal{I}_\varphi = 0$ must be topologically obstructed since the Chern-vorticity theorem indicates a nonzero vorticity $\nu = C_1 + C_2 = 2\text{sgn}(\mu)$. $\mathcal{I}_\varphi = 0$ is automatically satisfied if we consider only pairings proportional to $\sigma_{x,y}$, i.e., only $d_x(\mathbf{k})$ and $d_y(\mathbf{k})$ are nonzero in $\Delta(\mathbf{k})$. To see this, note that the normal states over the equator of the Fermi surface, $|\xi_\pm^{(e)}(k_z = 0)\rangle$, must be eigenstates of σ_z, since $h_0|_{k_z=0} \propto \sigma_z$. As a result, any $\Delta(\mathbf{k}) \sim \sigma_{x,y}$ will consistently vanish on the equator upon projection onto $\mathcal{M}_\pm$, which makes the equator effectively a point even after introducing the pairing. Therefore, the boundary term will vanish. Meanwhile, the $\sigma_\pm$ component of $\Delta(\mathbf{k})$ can contribute to $\mathcal{I}_\varphi$ by the winding phase of d_+ (d_-) around the equator for $\mu > 0$ ($\mu < 0$), so long as $d_\pm(k_z = 0) \neq 0$ and thus the equator can no longer be viewed as a point after introducing the pairing. Here, we have defined $\sigma_\pm = (\sigma_0 \pm \sigma_z)/2$ and $d_\pm(\mathbf{k}) = d_0(\mathbf{k}) \pm d_z(\mathbf{k})$. To generally understand the topological obstruction when I_φ is nonzero, we summarize the symmetric pairing channels (i.e., pairing terms that form representations of the C_{4h} group) up to second order in momentum in Table. I. Based on Table. I, it is straightforward to see that A_u and B_u pairings are the only two pairing channels that can contribute to $\mathcal{I}_\varphi$. Since $d_\pm(\mathbf{k})$ must be an odd function of $k_\pm = k_x \pm ik_y$ for both A_u and B_u irreps, the corresponding phase winding of $d_\pm$ around the equator must be $(4m+1)$ times of 2π with $m \in \mathbb{Z}$ [22]. This necessarily leads to a non-zero odd-integer-valued ν for all relevant A_u and B_u pairings. Since all pairings with $\mathcal{I}_\varphi = 0$ feature $\nu = 2$ and all pairings with $\mathcal{I}_\varphi \neq 0$ have ν to be odd, we conclude that all intra-FS pairing channels for the Berry-dipole FS are obstructed and nodal.

As a concrete example, let us focus on $\Delta = d_x(\mathbf{k})\sigma_x$ to explicitly illustrate the dipole-induced obstruction and relegate the discussions on other pairing channels in the SM [22]. We set $\Sigma = 0$ and the FS at $\mu \neq 0$ is a sphere of radius $\sqrt{|\mu|}$, which can be parameterized by a polar angle $\theta \in [0, \pi]$ and an azimuthal angle $\phi \in [0, 2\pi)$. For $\mu < 0$, we find the electron wavefunction to be $|\xi^{(e,I)}(\mathbf{k})\rangle = (-\cos\theta e^{-i\phi}, \sin\theta)^T$, which is a constant spinor $(0,1)^T$ at the equator. Under this gauge choice, $\mathcal{M}_\pm$ are both effectively closed, while $|\xi^{(e,I)}(\mathbf{k})\rangle$ becomes singular at the north pole ($\theta = 0$). This implies an obstruction to define a globally smooth gauge, thanks to the non-zero Chern number on each hemisphere.

A_g	B_g	${}^1E_g$	${}^2E_g$	A_u	B_u	${}^1E_u$	${}^2E_u$
$(k_x^2 - k_y^2)\sigma_y$	$\Delta_0\sigma_y$	$k_z k_-\sigma_y$	$k_z k_+\sigma_y$	$k_\pm\sigma_\pm$	$k_\mp\sigma_\pm$	$k_z\sigma_-$	$k_z\sigma_+$
$k_x k_y\sigma_y$					$k_z\sigma_x$	$k_-\sigma_x$	$k_+\sigma_x$

TABLE I. Pairing classification for Berry-dipole FS following the C_{4h} irreps. For B_g-pairing, $d_y = \Delta_0$ is a constant.

To ensure the wavefunction is merely locally singular, we consider $|\xi^{(e,I)}(\mathbf{k})\rangle$ for $\theta \in [\frac{\pi}{4}, \frac{3\pi}{4}]$, and choose a different gauge choice for $\theta \in [0, \frac{\pi}{4}] \cup [\frac{3\pi}{4}, \pi]$ with $|\xi^{(e,II)}(\mathbf{k})\rangle = (-\cos\theta, \sin\theta e^{i\phi})^T$. Straightforward calculations lead to:

$$\Delta_{\text{eff}}^{(I)} = d_x e^{i\phi}\sin 2\theta, \quad \Delta_{\text{eff}}^{(II)} = d_x e^{-i\phi}\sin 2\theta. \tag{6}$$

Apparently, Δ_{eff} features two zeros on $\mathcal{M}_+$, one at the north pole and another at the equator. Based on the form of $\Delta_{\text{eff}}^{(II)}$, it is easy to see that the vorticity of the north-pole zero is $\nu_0 = -1$. Meanwhile, the vorticity for the equator zero is also -1, which can be achieved by performing a *clockwise* loop integral of the phase of $\Delta_{\text{eff}}^{(I)}$ at $\theta = \frac{\pi}{2} - \epsilon$ [22]. Together, we find the net vorticity $\nu = -2$ for $\mathcal{M}_+$, which is consistent with the prediction of the Chern-vorticity theorem.

We now make a few remarks. First of all, the vorticity-induced pairing zeros always exist, regardless of the detailed form of $d_x(\mathbf{k})$. The zeros of $d_x(\mathbf{k})$ itself may lead to additional zeros of Δ_{eff}, beyond the topologically obstructed ones. Second, we highlight that the counting of ν for intra-FS pairing does depend on a special gauge choice with which $\mathcal{M}_\pm$ are effectively closed. Crucially, M_z symmetry guarantees the existence of such a gauge in our case [22], ensuring the ν counting is always possible. Apparently, the nodal structure of Δ_{eff} must be gauge-invariant. Therefore, applying the Chern-vorticity theorem under a proper gauge thoroughly informs the obstructed pairing zeros that are gauge-independent.

Finally, let us take the ${}^2E_u$ pairing $d_x(\mathbf{k}) = k_+$ as an example to numerically explore the nodal nature of the obstructed SC phases. In Fig. 2, we plot the pairing gap function on the corresponding FS and track its evolution as a function of Σ and μ, where the BdG Weyl nodes and nodal loops are highlighted in black. When $|\mu| > |\Sigma|$, we find a single sphere-like FS for both NLSM ($\Sigma < 0$) and WSM ($\Sigma > 0$), which exhibits both a BdG nodal loop at the equator and a pair of BdG Weyl nodes at the poles. This directly follows our analysis of vorticity counting. Further reducing $|\mu|$ triggers a Lifshitz transition for NLSM, which makes the point nodes merge. Surprisingly, the merging of these oppositely charged Weyl nodes leads to a second nodal loop at $k_z = 0$. This is in

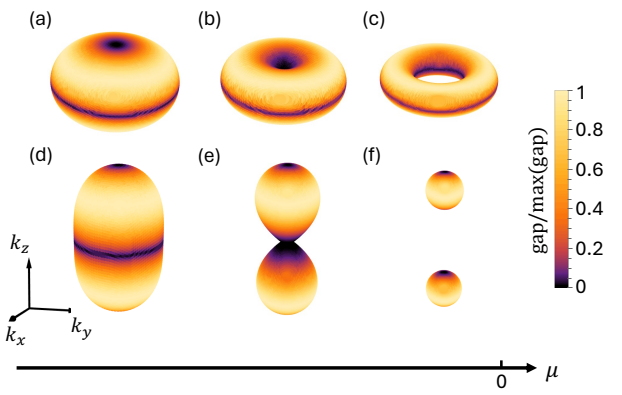


FIG. 2. Superconducting gap on the FS. (a)-(c) shows the projected pairing gap for NLSM ($\Sigma = -0.1$) with $\mu = -0.2, -0.1, -0.05$, respectively. (d)-(f) shows the projected pairing gap for WSM ($\Sigma = 0.1$) with $\mu = -0.2, -0.1, -0.05$, respectively. Note that a Lifshitz transition occurs at $|\mu| = |\Sigma|$ where the number of FSs changes.

contrast with the expected pair annihilation process in conventional Weyl SCs, as shown in the SM [22]. Meanwhile, a similar Lifshitz transition for WSM shrinks the BdG nodal loop to a point, which further splits into a pair of Weyl nodes. This robust conversion between Weyl nodes and nodal loops for the BdG bands directly arises from the effective closedness of $\mathcal{M}_\pm$ [22], which is reminiscent of similar behaviors in its normal state h_0 [26].

Application to $j = 3/2$ SCs. — As a real-world example, we now demonstrate that the BdG line nodes of half-Heusler-based $j = 3/2$ SCs such as YPtBi and LuPdBi are deeply rooted in the mechanism of dipole obstruction.

We start with a generalized Luttinger-Kohn Hamiltonian as a normal state of interest [30, 31],

$$h_L^{(\alpha)}(\mathbf{k}) = -\sqrt{3}\alpha(k_x^2 - k_y^2)\gamma_1 - 2\sqrt{3}\alpha k_x k_y \gamma_2 - 2\sqrt{3}k_z k_x \gamma_3 - 2\sqrt{3}k_z k_y \gamma_4 + M(\mathbf{k})\gamma_5, \quad (7)$$

where $\gamma_1 = \tau_x\sigma_0$, $\gamma_2 = \tau_y\sigma_0$, $\gamma_3 = \tau_z\sigma_x$, $\gamma_4 = \tau_z\sigma_y$, $\gamma_5 = \tau_z\sigma_z$, and $M(\mathbf{k}) = k_x^2 + k_y^2 - 2k_z^2$. τ's and σ's represent the Pauli matrix for electrons' orbital and spin. When $\alpha = 1$, $h_L^{(1)}$ recovers the standard isotropic Luttinger semimetal, which nicely captures the low-energy normal state of general $j = 3/2$ half-Heusler SCs. While several candidate pairing channels have been theoretically proposed [32–38], a recent experiment reports a doping-dependent nodeless-to-nodal transition in LuPdBi [20]. This observation strongly supports the mixed-parity singlet-septet pairing $\tilde{\Delta}(\mathbf{k}) = \tilde{\Delta}_s + \tilde{\Delta}_p$ [21], with $\tilde{\Delta}_s = i\Delta_s\tau_x\sigma_y$ and

$$\tilde{\Delta}_p = \Delta_p\Big(\frac{3}{4}k_-\tau_z\sigma_+ + \frac{3}{4}k_+\tau_z\sigma_- + \frac{\sqrt{3}}{2}k_z\tau_0\sigma_x + \frac{\sqrt{3}}{4}k_+\tau_x\sigma_+ - \frac{\sqrt{3}}{4}k_-\tau_x\sigma_-\Big), \quad (8)$$

which belongs to the A_1 irrep of T_d group. Specifically, with just $\tilde{\Delta}_p$, the BdG spectrum of $h_L^{(1)}$ displays point nodes at $k_{x,y,z}$ axes [c.f. Fig. 3(b)]. Turning on $\tilde{\Delta}_s$ further inflates the point nodes into nodal loops, eventually leading to a full gap when $\tilde{\Delta}_s$ dominates. However, why the p-wave pairing can lead to point nodes can be quite puzzling. For example, let us set $\Delta_s = 0$ and focus on the BdG physics along the k_z axis. While $\tilde{\Delta}_p \sim k_z\tau_0\sigma_x \neq 0$ for $k_z \neq 0$, the existence of point nodes implies that the projection of $\tilde{\Delta}_p(0, 0, k_z)$ onto the FS must vanish.

To trace the origin of these point nodes, we note that when $\alpha = 0$, $h_L^{(0)}(\mathbf{k}) \sim \tau_z \otimes h_0(\mathbf{k})$ exactly describes a *Dirac-dipole semimetal* [39] that comprises two decoupled copies of the Berry-dipole Hamiltonian at $\Sigma = 0$, up to some parameter rescaling. The block-diagonal nature of $h_L^{(0)}(\mathbf{k})$ suggests an emergent pseudospin conservation symmetry $U(1)_s$ generated by $S_z = \tau_z\sigma_0$, with which the two Berry-dipole blocks are carrying opposite spins. Note that an $\alpha \neq 0$ generally reduces $U(1)_s$ to the time-reversal symmetry $\mathcal{T} = i\tau_x\sigma_y\mathcal{K}$, with $\mathcal{K}$ the complex conjugation. Besides, $h_L^{(0)}(\mathbf{k})$ fully inherits the C_{4h} symmetry of h_0 with an updated rotation generator $J_z = \mathrm{diag}(\frac{3}{2}, \frac{1}{2}, -\frac{1}{2}, -\frac{3}{2})$ and $M_z = i\tau_0\sigma_z$. For a finite μ, the Dirac-dipole semimetal features a pair of decoupled FSs, one for each spin sector. Hence, all intra-FS pairings are intra-spin pairings, and vice versa.

Notably, the first three terms of $\tilde{\Delta}_p(\mathbf{k})$ describe the intra-spin pairing process. Within each spin sector, these pairings correspond to the B_u pairings in Table I, all of which are hence *dipole-obstructed* for $h_L^{(0)}(\mathbf{k})$. Applying the Chern-vorticity theorem in Eq. 2, we find this set of intra-spin pairing terms to carry a nontrivial pairing vorticity of $\nu = -1$ [22], which strictly enforces pairing zeros (or equivalently point nodes) on both the north and south poles of the FS. Meanwhile, the remaining pairing terms of $\tilde{\Delta}_p(\mathbf{k})$ are inter-spin and exhibit no obvious vortex pattern. Nonetheless, both inter-spin pairings vanish on the k_z axis and their existence is thus invisible to the dipole-obstructed pairing zeros. This is not a coincidence – actually the dipole-obstructed pairing zeros for the intra-spin pairings are robust against most $C_{4h} \times \mathcal{T}$ symmetric inter-spin pairings as discussed in Supplementary Material S5. Therefore, the nodal structures in Dirac dipole semimetals originate from dipole-obstructed intra-spin pairing and remain robust in the presence of symmetric inter-spin pairing. In this sense, we refer to such nodal structures as having a dipole-obstructed origin. In Fig. 3(a), we numerically confirm the predicted pairing zeros of $\tilde{\Delta}_p(\mathbf{k})$ by mapping out the pairing gap on the FS of the Dirac-dipole semimetal.

We now revisit the isotropic limit ($\alpha = 1$) that the $j = 3/2$ SCs follow. Since all α-relevant terms in $h_L^{(\alpha)}$ vanish on the k_z axis due to the four-fold rotation symmetry along z-direction, turning on α will *not* disrupt the obstructed pairing zeros in the Dirac-dipole limit. In another word, the nodal structures observed in Dirac-dipole semimetals are robust against the α-relevant terms and persist in the $j = 3/2$ SCs at $\alpha = 1$. Moreover, $h_L^{(1)}(\mathbf{k})$ respects a larger symmetry group (e.g., T_d) than that of

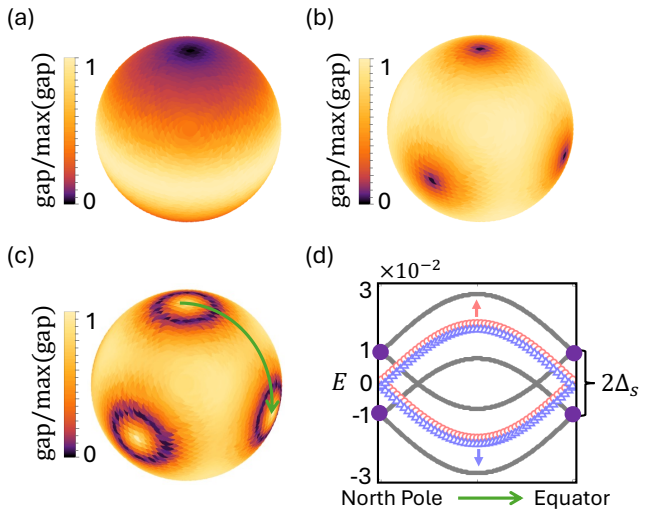


FIG. 3. Superconducting gap over the FS of (a) a Dirac-dipole semimetal ($\alpha = 0$); (b) a Luttinger semimetal ($\alpha = 1$) with $(\Delta_s, \Delta_p) = (0, 0.05)$; and (c) a Luttinger semimetal with $(\Delta_s, \Delta_p) = (0.01, 0.05)$, at $\mu = -0.2$. (d) Spectrum along a path on FS indicated by the green arrow in (c). The red and blue markers depict the spin-degenerate spectrum shown in (b) along the path, while the gray markers represent the spectrum plotted in (c) along the path, where spin degeneracy is lifted by s-wave pairing. The purple dots highlight the band degeneracies induced by the dipole obstruction.

$h_L^{(0)}(\mathbf{k})$, which features a three-fold rotation $C_{3,111}$ that permutes k_x, k_y, and k_z. Hence, BdG point nodes should also emerge at both k_x and k_y axes, which is explicitly confirmed in Fig. 3(b). In other words, $C_{3,111}$ enables us to designate any of the $k_{x,y,z}$-axes as the C_4-rotation axis for the previous Dirac-dipole discussion. In this case, *all of the six p-wave-induced point nodes for $j = 3/2$ SCs have a dipole-obstructed origin.*

Finally, let us turn on a subdominant $\tilde{\Delta}_s$ to achieve the BdG line nodes, as shown in Fig. 3(c). Specifically, the effect of $\tilde{\Delta}_s$ is to lift the degeneracy of FSs by breaking the inversion symmetry, causing the one band to shift upward and another band to shift downward, as shown in Fig. 3(d). When this degeneracy lifting is small, it generally leads to accidental inter-FS band crossings that manifest as line nodes. The opposite energy shift can be clearly understood through symmetry analysis. Interested readers can find the detailed explanation in the Supplementary Material (SM) [22]. While the dipole-obstructed pairing [purple dots in Fig. 3(d)] now show up at a finite energy $E = \pm\tilde{\Delta}_s$, their existence ensures the BdG line nodes to necessarily show up even for an arbitrarily small $\tilde{\Delta}_s$. Note that we have omitted a small asymmetric spin-orbit coupling (ASOC) term in Eq. 7, which is intrinsic to zinc-blende materials. While the ASOC is key to mixing s and p-wave pairings, its effect on the BdG band spectrum is similar to that of the s-wave pairing. A detailed discussion on the ASOC term can be found in the SM [22].

Discussions.— To summarize, we have established a general theoretical framework for comprehending topologically obstructed nodal pairing over a single FS. This leads us to uncover a class of Berry-dipole FSs where the SC state induced by any intra-FS pairing will be dipole-obstructed and nodal. The hidden Berry-dipole physics in the Luttinger-Kohn model further motivates us to explore the $j = 3/2$ pairings in half-Heusler SCs. Focusing on the singlet-septet pairing channel, we find that the dipole obstruction contributes significantly to the BdG line nodes observed in experiments. Notably, Berry and Dirac dipoles, as well as Luttinger semimetals, have been recently established as critical points for delicate topological phases [16, 31, 39],. Therefore, our dipole-obstructed pairing offers the first example of how delicate topological bands can decisively impact the correlated electronic orders in real-world quantum materials.

We emphasize that our Chern-vorticity theorem goes beyond SCs and applies to general electronic orders such as charge-density waves, excitons, magnetism, etc. It would be interesting to explore possible dipole-obstructed phenomena in other non-superconducting Luttinger semimetals such as HgTe [40] and $Pr_2Ir_2O_7$ [41]. Besides, we find many inter-spin pairings for the $j = 3/2$ system to feature emergent nodal structures in the BdG spectrum, despite carrying no vortex structure. As elaborated in the SM [22] for the Dirac-dipole model, these "unobstructed" pairing zeros arise from the geometric textures of the Bloch states on the FSs, which are beyond the scope of the Chern-vorticity theorem. How to interpret these geometry-relevant nodal pairings is an absolutely intriguing question for future research.

ACKNOWLEDGMENTS

We thank J. Yu, Y. Wang, L.-H. Hu, A. Alexandradinata, and Y.-M. Lu for helpful discussions. P.Z was primarily supported by the Center for Emergent Materials, an NSF MRSEC, under award number DMR-2011876. R.-X.Z. is supported by a start-up fund of the University of Tennessee.

REFERENCES

[1] J. Bardeen, L. N. Cooper, and J. R. Schrieffer, Microscopic theory of superconductivity, Phys. Rev. **106**, 162 (1957).
[2] M. Sigrist and K. Ueda, Phenomenological theory of unconventional superconductivity, Rev. Mod. Phys. **63**, 239 (1991).
[3] C. C. Tsuei and J. R. Kirtley, Pairing symmetry in cuprate superconductors, Rev. Mod. Phys. **72**, 969 (2000).
[4] H. Kim, K. Wang, Y. Nakajima, R. Hu, S. Ziemak, P. Syers, L. Wang, H. Hodovanets, J. D. Denlinger, P. M. Brydon, *et al.*, Beyond triplet: Unconventional supercon-

ductivity in a spin-3/2 topological semimetal, Science advances **4**, eaao4513 (2018).
[5] A. Damascelli, Z. Hussain, and Z.-X. Shen, Angle-resolved photoemission studies of the cuprate superconductors, Rev. Mod. Phys. **75**, 473 (2003).
[6] O. Fischer, M. Kugler, I. Maggio-Aprile, C. Berthod, and C. Renner, Scanning tunneling spectroscopy of high-temperature superconductors, Rev. Mod. Phys. **79**, 353 (2007).
[7] R. Prozorov and R. W. Giannetta, Magnetic penetration depth in unconventional superconductors, Superconductor Science and Technology **19**, R41 (2006).
[8] S. Murakami and N. Nagaosa, Berry phase in magnetic superconductors, Phys. Rev. Lett. **90**, 057002 (2003).
[9] Y. Li and F. D. M. Haldane, Topological nodal cooper pairing in doped weyl metals, Phys. Rev. Lett. **120**, 067003 (2018).
[10] Y. Wang and P. Ye, Topological density-wave states in a particle-hole symmetric weyl metal, Phys. Rev. B **94**, 075115 (2016).
[11] E. Muñoz, R. Soto-Garrido, and V. Juričić, Monopole versus spherical harmonic superconductors: Topological repulsion, coexistence, and stability, Phys. Rev. B **102**, 195121 (2020).
[12] J. Yu, Y.-A. Chen, and S. Das Sarma, Euler-obstructed cooper pairing: Nodal superconductivity and hinge majorana zero modes, Phys. Rev. B **105**, 104515 (2022).
[13] J. Yu, M. Xie, F. Wu, and S. Das Sarma, Euler-obstructed nematic nodal superconductivity in twisted bilayer graphene, Phys. Rev. B **107**, L201106 (2023).
[14] Y.-J. Wang, G.-D. Zhou, S.-Y. Peng, B. Lian, and Z.-D. Song, Molecular pairing in twisted bilayer graphene superconductivity, arXiv preprint arXiv:2402.00869 (2024).
[15] C. Sun and Y. Li, $\mathbb{Z}_2$ topologically obstructed superconducting order, arXiv preprint arXiv:2009.07263 (2020).
[16] A. Nelson, T. Neupert, A. Alexandradinata, and T. c. v. Bzdušek, Delicate topology protected by rotation symmetry: Crystalline hopf insulators and beyond, Phys. Rev. B **106**, 075124 (2022).
[17] N. P. Butch, P. Syers, K. Kirshenbaum, A. P. Hope, and J. Paglione, Superconductivity in the topological semimetal yptbi, Phys. Rev. B **84**, 220504 (2011).
[18] Y. Nakajima, R. Hu, K. Kirshenbaum, A. Hughes, P. Syers, X. Wang, K. Wang, R. Wang, S. R. Saha, D. Pratt, *et al.*, Topological r pdbi half-heusler semimetals: A new family of noncentrosymmetric magnetic superconductors, Science advances **1**, e1500242 (2015).
[19] O. Pavlosiuk, D. Kaczorowski, and P. Wiśniewski, Shubnikov-de haas oscillations, weak antilocalization effect and large linear magnetoresistance in the putative topological superconductor lupdbi, Scientific reports **5**, 9158 (2015).
[20] K. Ishihara, T. Takenaka, Y. Miao, Y. Mizukami, K. Hashimoto, M. Yamashita, M. Konczykowski, R. Masuki, M. Hirayama, T. Nomoto, R. Arita, O. Pavlosiuk, P. Wiśniewski, D. Kaczorowski, and T. Shibauchi, Tuning the parity mixing of singlet-septet pairing in a half-heusler superconductor, Phys. Rev. X **11**, 041048 (2021).
[21] P. M. R. Brydon, L. Wang, M. Weinert, and D. F. Agterberg, Pairing of $j = 3/2$ fermions in half-heusler superconductors, Phys. Rev. Lett. **116**, 177001 (2016).
[22] See the Supplemental Material for (i) a detailed proof of the Chern-vorticity theorem; (ii) detailed analysis for general pairings in Berry-dipole semimetals and inter-spin pairings in Dirac-dipole semimetals; and (iii) case studies on WSM, Berry dipole SC, and perturbations from ASOC.
[23] E. Bobrow, C. Sun, and Y. Li, Monopole charge density wave states in weyl semimetals, Phys. Rev. Res. **2**, 012078 (2020).
[24] N. Bultinck, S. Chatterjee, and M. P. Zaletel, Mechanism for anomalous hall ferromagnetism in twisted bilayer graphene, Phys. Rev. Lett. **124**, 166601 (2020).
[25] P. Zhu and A. Alexandradinata, Anomalous shift and optical vorticity in the steady photovoltaic current, arXiv preprint arXiv:2308.08596 (2023).
[26] X.-Q. Sun, S.-C. Zhang, and T. c. v. Bzdušek, Conversion rules for weyl points and nodal lines in topological media, Phys. Rev. Lett. **121**, 106402 (2018).
[27] A. Graf and F. Piéchon, Massless multifold hopf semimetals, Phys. Rev. B **108**, 115105 (2023).
[28] Z.-Y. Zhuang, C. Zhang, X.-J. Wang, and Z. Yan, Berry-dipole semimetals, arXiv preprint arXiv:2404.10049 (2024).
[29] A. C. Tyner and S. Sur, Dipolar weyl semimetals, Phys. Rev. B **109**, L081101 (2024).
[30] L.-H. Hu and R.-X. Zhang, Topological superconducting vortex from trivial electronic bands, Nature Communications **14**, 640 (2023).
[31] P. Zhu and R.-X. Zhang, Delicate topology of luttinger semimetal, arXiv preprint arXiv:2308.05793 (2023).
[32] W. Yang, T. Xiang, and C. Wu, Majorana surface modes of nodal topological pairings in spin-$\frac{3}{2}$ semimetals, Phys. Rev. B **96**, 144514 (2017).
[33] B. Roy, S. A. A. Ghorashi, M. S. Foster, and A. H. Nevidomskyy, Topological superconductivity of spin-3/2 carriers in a three-dimensional doped luttinger semimetal, Phys. Rev. B **99**, 054505 (2019).
[34] I. Boettcher and I. F. Herbut, Unconventional superconductivity in luttinger semimetals: Theory of complex tensor order and the emergence of the uniaxial nematic state, Phys. Rev. Lett. **120**, 057002 (2018).
[35] J. Yu and C.-X. Liu, Singlet-quintet mixing in spin-orbit coupled superconductors with $j = \frac{3}{2}$ fermions, Phys. Rev. B **98**, 104514 (2018).
[36] J. W. F. Venderbos, L. Savary, J. Ruhman, P. A. Lee, and L. Fu, Pairing states of spin-$\frac{3}{2}$ fermions: Symmetry-enforced topological gap functions, Phys. Rev. X **8**, 011029 (2018).
[37] P. Dutta, F. Parhizgar, and A. M. Black-Schaffer, Superconductivity in spin-3/2 systems: Symmetry classification, odd-frequency pairs, and bogoliubov fermi surfaces, Phys. Rev. Res. **3**, 033255 (2021).
[38] M. Bahari, S.-B. Zhang, and B. Trauzettel, Intrinsic finite-energy cooper pairing in $j = 3/2$ superconductors, Phys. Rev. Res. **4**, L012017 (2022).
[39] P. Zhu, A. Alexandradinata, and T. L. Hughes, $\mathbb{Z}_2$ spin hopf insulator: Helical hinge states and returning thouless pump, Phys. Rev. B **107**, 115159 (2023).
[40] R. Piotrzkowski, S. Porowski, Z. Dziuba, J. Ginter, W. Giriat, and L. Sosnowski, Band structure of hgte, physica status solidi (b) **8**, K135 (1965).
[41] T. Kondo, M. Nakayama, R. Chen, J. Ishikawa, E.-G. Moon, T. Yamamoto, Y. Ota, W. Malaeb, H. Kanai, Y. Nakashima, *et al.*, Quadratic fermi node in a 3d strongly correlated semimetal, Nature communications **6**, 10042 (2015).